Editors' Suggestion

Comprehensive *Ab Initio* Investigation of the Phase Diagram of Quasi-One-Dimensional Molecular Solids

Kazuyoshi Yoshimi,[1,*] Takahiro Misawa,[1,2,*] Takao Tsumuraya,[3,4] and Hitoshi Seo[5,6]
[1]Institute for Solid State Physics, University of Tokyo, 5-1-5 Kashiwanoha, Kashiwa, Chiba 277-8581, Japan
[2]Beijing Academy of Quantum Information Sciences, Haidian District, Beijing 100193, China
[3]Priority Organization for Innovation and Excellence, Kumamoto University, 2-39-1 Kurokami, Kumamoto 860-8555, Japan
[4]Magnesium Research Center, Kumamoto University, 2-39-1 Kurokami, Kumamoto 860-8555, Japan
[5]Condensed Matter Theory Laboratory, RIKEN, Wako, Saitama 351-0198, Japan
[6]Center for Emergent Matter Science (CEMS), RIKEN, Wako, Saitama 351-0198, Japan

(Received 18 October 2022; revised 23 May 2023; accepted 31 May 2023; published 18 July 2023)

An *ab initio* investigation of the family of molecular compounds TM_2X is conducted, where TM is either TMTSF or TMTTF and X takes centrosymmetric monovalent anions. By deriving the extended Hubbard-type Hamiltonians from first-principles band calculations and evaluating not only the intermolecular transfer integrals but also the Coulomb parameters, we discuss their material dependence in the unified phase diagram. Furthermore, we apply the many-variable variational Monte Carlo method to accurately determine the symmetry-breaking phase transitions, and show the development of the charge and spin orderings. We show that the material-dependent parameter can be taken as the correlation effect, represented by the value of the screened on-site Coulomb interaction U relative to the intrachain transfer integrals, for the comprehensive understanding of the spin and charge ordering in this system.

DOI: 10.1103/PhysRevLett.131.036401

Introduction.—Molecular solids serve as textbook materials to study many-body physics in condensed matter, despite their complex crystal structures with many atoms in the unit cell, owing to the success in modeling the low-energy electronic properties based on the frontier molecular orbitals [1,2]. A general challenge is to understand multiple symmetry-broken phases observed in different systems in a systematic way, where the charge, spin, and lattice degrees of freedom are coupled to each other, based on the effective Hamiltonians and identifying the factors governing them [3].

The family of compounds constituted by TMTSF (= tetramethyltetraselenafulvalene) or TMTTF (= tetramethyltetrathiafulvalene) molecules, which we call together TM here, forming 2 : 1 salts with monovalent anions X^{-1}, TM_2X, has been studied for decades as a typical example showing such a rich variety of phases [2–5]. TMTSF_2X historically stands as the first organic system undergoing superconductivity [6]. Unconventional superconductivity with an anisotropic gap function is realized, whose "glue" for the Cooper pair formation is the strong spin fluctuation, supported by the pressure-temperature phase diagram with the superconducting phase neighboring an antiferromagnetic (AFM) phase driven by the nesting of the Fermi surface [7–11].

Later, the isostructural TMTTF counterparts became realized as strongly correlated electron systems, owing to the atomic substitution resulting in smaller bandwidths than in the TMTSF compounds [5,12,13]. In particular, at high temperatures of the order of 100 K, TMTTF_2X hosts a competition between a Mott insulating state, the so-called dimer-Mott (DM) insulator, and a charge ordering (CO) state with electron-rich and poor molecules spontaneously arranging to avoid the Coulomb repulsion: a common framework for the understanding of correlated quarter-filled systems [14–16]. In the low-temperature region (∼10 K), on the other hand, where the magnetic interactions start to develop between the localized spins in the strongly correlated regime, the AFM state competes with the spin-Peierls instability accompanying lattice distortion owing to the quasi-one-dimensionality [17–19].

The variation among the symmetry-breaking states, in which both the charge and spin degrees of freedom are involved, depending on the applied pressure to the compounds and on the choice of the combination of TM and X (chemical pressure), has been extensively discussed [20–24]. Nevertheless, there is room toward a comprehensive understanding of them. There are different views on how the choice of X and the amount of applied pressure affect the microscopic parameters, and the impact of the difference between TMTSF and TMTTF is still obscure. Conventionally, the two systems are drawn in a unified pressure-temperature phase diagram [4,5,22,23], as shown in Fig. 1(a). Although there are different versions in the literature, here we simply draw the "ambient pressure" positions of the representative compounds in an equally spaced manner, together with the reported transition temperatures [13,25–28].

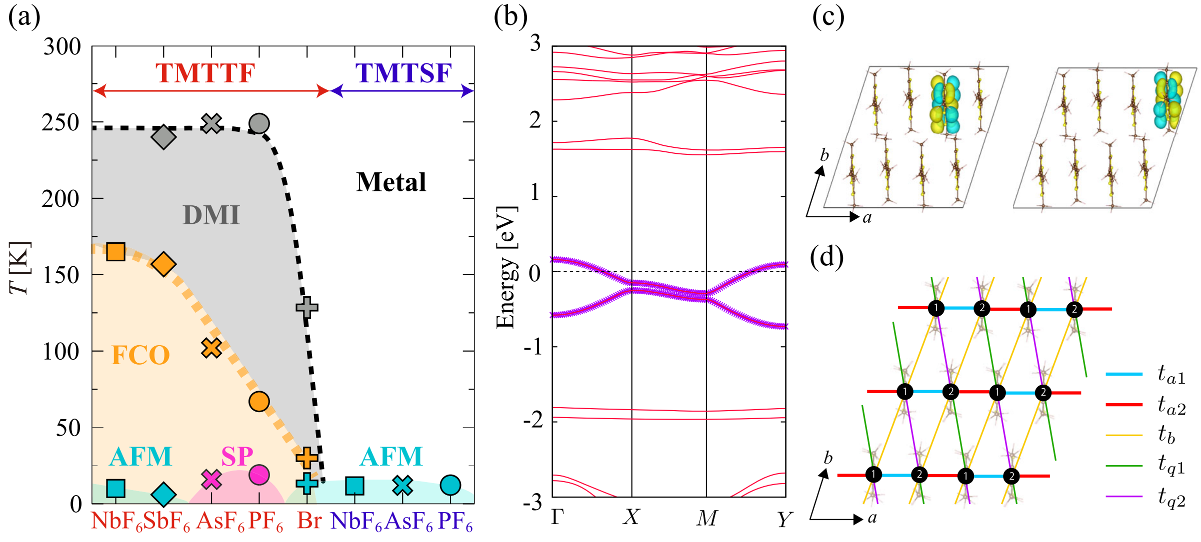

FIG. 1. (a) Schematic phase diagram of $(\mathrm{TM})_2X$. DMI, FCO, AFM, and SP indicate dimer-Mott insulating, ferroelectric charge ordered, antiferromagnetic, and spin-Peierls phases, respectively. Symbols are the ambient-pressure transition temperatures for each material [29]. We note that, since the reported AFM transition temperatures for the TMTSF salts are the same [29], the order is determined by the volume of the unit cell. (b) Band structure of $\mathrm{TMTTF_2PF_6}$. The thin solid lines are the DFT results, while the bold lines are obtained using the MLWFs, overlapping the valence bands. We set the Fermi energy to zero (the dotted line). (c) Drawings of the two MLWFs for $\mathrm{TMTTF_2PF_6}$. (d) Definition of the transfer integrals. The TMTTF molecules and MLWFs are drawn by using VESTA [34].

From the early days, in the TMTSF salts, it is discussed that the applied pressure increases the dimensionality [6]. On the other hand, the degree of dimerization along the one-dimensional chain direction was also pointed out to be an important factor, especially for the TMTTF salts [35]. And more recently, to understand the complicated interplay between the phases toward the left-hand end of the phase diagram, it was proposed that the CO instability can be the controlling factor [22]; this suggests the essential role of electron correlation. Whether we can choose a parameter that varies monotonically as we go along the compounds listed in the horizontal axis is the question we ask here.

In this Letter, to investigate these issues, we apply first-principles density functional theory (DFT) calculations [36,37] to a number of members of the TM_2X family with centrosymmetric X; we numerically derive not only the transfer integrals between the molecules but also the correlation parameters. We then use these parameters as inputs to a highly accurate numerical solver, i.e., the many-variable variational Monte Carlo (mVMC) method [38–40], for the effective extended Hubbard-type Hamiltonian and seek possible long-range ordering in the charge and spin degrees of freedom. As a result, we can directly compare with the experimentally observed phases and comprehensively extract the determining factor at a quantitative level.

Ab initio derivation of microscopic parameters.—The DFT calculations are performed using QUANTUM ESPRESSO (version 6.6) [41] for the experimental crystal structures [13]. We employ norm-conserving pseudopotentials based on the Vanderbilt formalism with plane-wave basis sets [42,43]. The exchange-correlation function used in this study is the generalized gradient approximation by Perdew, Burke, and Ernzerhof [44], which is commonly used for accurately describing electronic states of molecular compounds [45]. The cutoff energies for plane waves and charge densities are 70 and 280 Ry, respectively. A $7 \times 7 \times 3$ uniform $\boldsymbol{k}$-point mesh was used with a Gaussian smearing method during self-consistent loops.

For deriving the interaction parameters, we use the constrained random phase approximation (cRPA) method [46,47]. In fact, previous studies applying the cRPA method to molecular solids show good agreement between the results for the derived effective Hamiltonians and the experiments [48–53]. On the basis of the obtained DFT electronic states, we construct maximally localized Wannier functions (MLWFs) and derive the parameters using RESPACK [54]. In the calculations, the energy cutoff for the dielectric function was set to be 3 Ry.

Figures 1(b) and 1(c) show the band structure and the MLWFs, respectively, of $\mathrm{TMTTF_2PF_6}$ as an example. The two bands crossing the Fermi energy are constituted from the bonding and antibonding combination of the highest occupied molecular orbitals situated on the two TMTTF molecules in the unit cell shown in Fig. 1(b). Using these MLWFs, we evaluated the transfer integrals and the density-density interactions, i.e., the on-site and off-site Coulomb interactions (the exchange interactions are negligibly small, so we omit them in the following). The obtained microscopic parameters are listed in Table II in the Supplemental Material [29]. We adopt the indices of bonds from Refs. [22,55], as shown in Fig. 1(d).

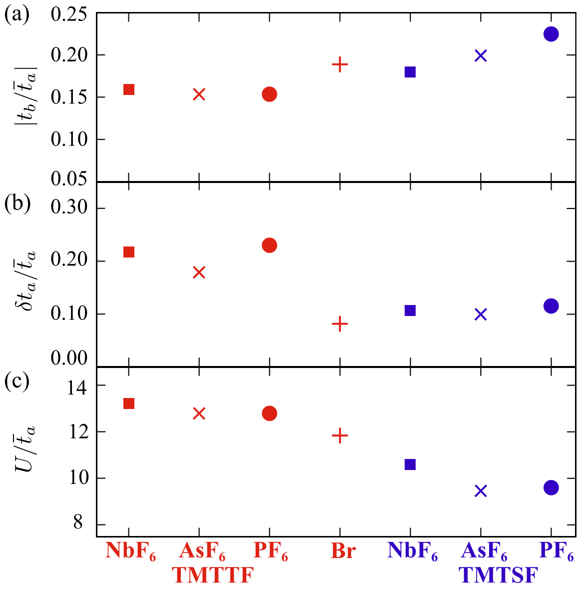

FIG. 2. (a) Transfer integral between TM molecules along b axis (t_b), (b) difference in the alternating transfer integrals along a axis ($\delta t_a \equiv |t_{a2} - t_{a1}|$), and (c) the on-site Coulomb interaction (U) for TM$_2X$ (TM = TMTSF, TMTTF, X = NbF$_6$, AsF$_6$, Br, and PF$_6$). Each value is normalized by the mean a-axis transfer integral, $\bar{t}_a \equiv |(t_{a1} + t_{a2})/2|$.

Then the following *ab initio* extended Hubbard-type Hamiltonian is obtained:

$$H = \sum_{ij,\sigma} t_{ij}(c^\dagger_{i\sigma} c_{j\sigma} + \mathrm{H.c.}) + U \sum_i n_{i\uparrow} n_{i\downarrow} + \sum_{ij} V_{ij} N_i N_j \tag{1}$$

where $c^\dagger_{i\sigma}$ and $c_{i\sigma}$ are the creation and annihilation operators of an electron with spin σ at the ith site, respectively. The number operators are defined as $n_{i\sigma} = c^\dagger_{i\sigma} c_{i\sigma}$ and $N_i = n_{i\uparrow} + n_{i\downarrow}$. t_{ij}, U, and V_{ij} represent the transfer integrals, on-site and off-site Coulomb interactions, respectively. We note that, although TM$_2X$ show quasi-one-dimensional electronic band structures, the Coulomb parameters show large values also for the interchain bonds.

First, let us discuss the material dependence of intermolecular transfer energies based on our evaluation. Since it is known that the temperature variation of structural parameters is large [56], here we show the results for TMTTF$_2X$ with X = NbF$_6$, AsF$_6$, Br, and PF$_6$ at fixed 200 K, and for TMTSF$_2X$ with X = NbF$_6$, AsF$_6$, and PF$_6$ at room temperature [29]. In Fig. 2, we show the variation of three different values along the horizontal axis of the phase diagram in Fig. 1(a). The first two, the degree of interchain couplings and the degree of dimerization plotted in Figs. 2(a) and 2(b), respectively, have been discussed in the literature as mentioned above. We renormalize them by the mean transfer integral along the a axis, $\bar{t}_a \equiv |(t_{a1} + t_{a2})/2|$, which is larger than those along the other directions.

The largest interchain transfer integral, which is t_b, is plotted in Fig. 2(a); the interlayer transfer integrals along the c axis are negligible. Our results show larger $|t_b/\bar{t}_a|$ for the TMTSF salts than the TMTTF salts as a general trend; TMTSF has a broader extent of the wave function in the transverse direction than TMTTF, owing to the difference between the Se and S atoms at the sides of the molecules. As for the degree of dimerization, $\delta t_a/\bar{t}_a \equiv |t_{a2} - t_{a1}|/\bar{t}_a$ [Fig. 2(b)], the overall tendency is that it decreases from the left to the right side, while some deviate from the monotonic variation; for example, TMTTF$_2$Br shows a similar value to the TMTSF salts.

Finally, Fig. 2(c) shows the on-site Coulomb interaction, U, which is a measure of the strength of electron correlation. The intermolecular parameters, V_{ij}, also show similar tendencies. We can see that $U/\bar{t}_a$ monotonically decrease from the left to the right side, except for the two salts at the right end: TMTSF$_2$PF$_6$ ($U/\bar{t}_a = 9.59$) is slightly larger than TMTSF$_2$AsF$_6$ ($U/\bar{t}_a = 9.46$). Since the electron correlation is responsible for all the phases, from the strongly correlated DM insulating and CO phases, to the nesting-driven AFM and the spin-fluctuation mediated superconducting phases, this behavior is consistent with the temperature scale for their occurrence, decreasing from left to right of the phase diagram in Fig. 1(a).

This tendency in $U/\bar{t}_a$ can be understood by the effect of chemical pressure. More concretely, first, by the unit cell volume decreasing from left to right, the transfer integrals reflecting the overlap between MLWFs increase. Next, since the screening effect becomes stronger with an increase of the band width, the screened U is smaller with an increase of the pressure. As a combination of them, together with the difference in the bare on-site Coulomb parameter U_{bare} between the molecules, $U/\bar{t}_a$ monotonically decreases from left to right in Fig. 2(c). For more detailed information about the parameters and their numerical accuracy, see the Supplemental Material [29].

mVMC analysis.—To directly detect the symmetry-breaking phase transitions, we solve the *ab initio* effective Hamiltonian by using the mVMC method [38–40]. The form of the variational wave function used in this study is given by

$$|\psi\rangle = \mathcal{L}_S \mathcal{P}_G \mathcal{P}_J |\phi_{\mathrm{pair}}\rangle, \tag{2}$$

where $\mathcal{P}_G$ ($\mathcal{P}_J$) represents the Gutzwiller factor [57] (Jastrow factor [58]) and $\mathcal{L}_S$ is the total spin projection. We use the spin singlet total spin projection ($S = 0$) for the ground states. The pair-product wave function $|\phi_{\mathrm{pair}}\rangle$ is defined as

$$|\phi_{\mathrm{pair}}\rangle = \left[\sum_{i,j=1}^{N_s} f_{ij} c^\dagger_{i\uparrow} c^\dagger_{j\downarrow}\right]^{N_e/2} |0\rangle, \tag{3}$$

where f_{ij} represents the variational parameters, and N_s and N_e are the number of sites and electrons, respectively. In the mVMC calculations, we map the lattice structure shown in Fig. 1(d) onto the square lattice without loss of generality. The total number of sites is given by $N_s = L_x \times L_y$. We impose a 4×2 sublattice structure and the periodic boundary conditions, and optimize all the variational parameters simultaneously using the stochastic reconfiguration method [38,59] to obtain the ground state.

We consider all the bonds that are listed in Table II in the Supplemental Material [29]; they contain all the bonds shown in Fig. 1(d) as well as V_{2a} that is the next-nearest-neighbor Coulomb interaction along the chain direction. We note that the effective Coulomb interactions are reduced by a constant shift $\Delta_{\mathrm{DDF}} = 0.20$ eV, adopting the results of the previous study [60,61], to take into account dimensional screening effects. We calculate the spin and charge structure factors defined as

$$N(\boldsymbol{q}) = \frac{1}{N_s} \sum_{i,j} \langle N_i \cdot N_j \rangle e^{i\boldsymbol{q}(\boldsymbol{r}_i - \boldsymbol{r}_j)}, \tag{4}$$

$$S(\boldsymbol{q}) = \frac{1}{N_s} \sum_{i,j} \langle \boldsymbol{S}_i \cdot \boldsymbol{S}_j \rangle e^{i\boldsymbol{q}(\boldsymbol{r}_i - \boldsymbol{r}_j)}, \tag{5}$$

where N_i ($\boldsymbol{S}_i$) represents the number (spin) operator at site i. The Fourier transformation is performed for the mapped square lattice.

Let us present $S(\boldsymbol{q})$ and $N(\boldsymbol{q})$ for the two end members of the phase diagram, TMTTF$_2$NbF$_6$ and TMTSF$_2$PF$_6$. As shown in Figs. 3(a) and 3(b), for TMTTF$_2$NbF$_6$, which has the strongest electronic correlation, the spin (charge) structure factors have a sharp peak at $\boldsymbol{q}^{\mathrm{spin}}_{\mathrm{peak}} = (\pi/2, \pi)$ [$\boldsymbol{q}^{\mathrm{charge}}_{\mathrm{peak}} = (\pi, 0)$]. The corresponding ordering pattern in the real space is shown in the inset of Fig. 3(a). Since these peak values remain finite after size extrapolation, the CO state with spin ordering is the ground state, consistent with previous studies [14,22]. Note that, in the previous studies the long range Coulomb interactions are introduced by hand to stabilize the CO state with the ferroelectric pattern which is observed experimentally. We emphasize that, here the condition favoring the ferroelectric CO state is satisfied from the *ab initio* way, displayed in Fig. S1(d) in the Supplemental Material [29]. In contrast, we find that the peak values of the structure factors for parameters of TMTSF$_2$PF$_6$ become significantly small as shown in Figs. 3(c) and 3(d). This result is consistent with our results above, that TMTSF$_2$PF$_6$ has much weaker electronic correlation.

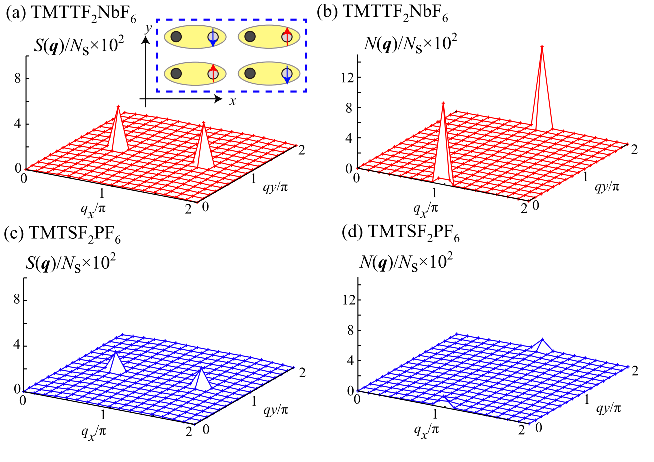

FIG. 3. Spin [$S(\boldsymbol{q})$] and charge [$N(\boldsymbol{q})$] structure factors for (a), (b) TMTTF$_2$NbF$_6$ and (c),(d) TMTSF$_2$PF$_6$ for $L_x = L_y = 16$. In the inset, we show the schematic spin and charge-ordered pattern of TMTTF$_2$NbF$_6$ in the real space, where the yellow oval represents the dimer. The broken blue line represents the 4×2 sublattice structure used in mVMC calculations.

To clarify the material dependence, we perform the mVMC calculations for all the members and conduct the size extrapolation for the obtained peak values, in the spin and charge structure factors, as shown in Figs. 4(a) and 4(b), respectively. The thermodynamic limits are defined as $M = \lim_{N_s \to \infty} S(\boldsymbol{q}^{\mathrm{spin}}_{\mathrm{peak}})/N_s$, $C = \lim_{N_s \to \infty} N(\boldsymbol{q}^{\mathrm{charge}}_{\mathrm{peak}})/N_s$. Both the spin and charge structure factors show nearly linear dependencies as a function of the linear dimension of the number of sites, i.e., $N_s^{1/2}$.

The material dependence of M and C is shown in Figs. 4(c) and 4(d), respectively, as a function of the

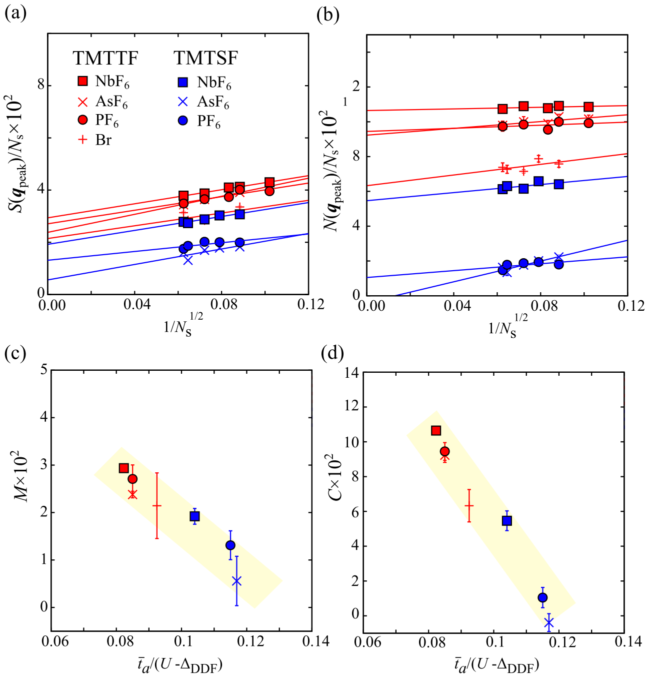

FIG. 4. Size dependence of (a) the spin and (b) the charge structure factors for five TMTTF salts and three TMTSF salts. Coulomb interaction dependence of the order parameter of (c) the spin ordering and (d) the charge ordering. Both the charge and spin order gradually decrease as a function of the Coulomb interaction.

inverse of the normalized Coulomb interaction, $(U - \Delta_{\mathrm{DDF}})/\bar{t}_a$. We find that the amplitude of the charge and spin orders decreases monotonically with respect to the amplitude of the Coulomb interactions. This tendency is consistent with the experimental results where the transition temperature of CO decreases by varying the material from left to right. At the border, $\mathrm{TMTSF_2AsF_6}$ and $\mathrm{TMTSF_2PF_6}$ show a small but finite value of M of the order of 10^{-2}, and C almost vanishes.

These results, combined with the *ab initio* results in Fig. 2(c), both clearly show that the charge and spin orderings are governed by the relative amplitude of the Coulomb interactions. This is the first *ab initio* evidence that the correlation effects play key roles in stabilizing the spin-charge ordering in TM_2X and serve as the good index for the horizontal axis of the unified phase diagram. The success here also indicates that our low-energy effective model is reliable at a quantitative level, considering the high precision of the mVMC method. This is owing to the fact that the band structure near the Fermi energy is simple, as shown in Fig. 1(b), which guarantees the accuracy of the cRPA method, since it incorporates the effect of bands other than the target bands. In fact, in many of the molecular solids, bands near the Fermi energy are isolated; thus it is expected that our approach can be applicable to a wide range of functional molecular materials.

Perspectives.—We have shown that the material dependence in the unified phase diagram for TM_2X is governed by the correlation effect, represented by the on-site Coulomb interaction U, which gives a comprehensive understanding of the spin and charge orderings in this system. One point that disagrees with the experiments is that in our results, spin patterns with long periodicity such as incommensurate AFM (spin-density-wave) states suggested experimentally are difficult to reproduce in our finite-size systems. Finally, superconductivity is not found in our study, which is consistent with experiments showing it under pressure for the compounds we studied; its *ab initio* investigation is left for future studies.

We thank R. Kato, S. Kitou, and T. Nakamura for fruitful discussions. This work was supported by MEXT/JSPJ KAKENHI under Grants No. 19K03723, No. 19K21860, No. 20H04463, No. 21H01041 No. 22K03526, No. 23H03818, and No. 23H04047. K. Y. and T. M. were supported by Building of Consortia for the Development of Human Resources in Science and Technology, MEXT, Japan. The computation in this work was performed using the facilities of the Supercomputer Center, Institute for Solid State Physics, University of Tokyo.

---

[*] These authors contributed equally to this work.

[1] T. Ishiguro, K. Yamaji, and G. Saito, *Organic Superconductors*, 2nd ed., Springer Series in Solid-State Sciences Vol. 88 (Springer, Berlin; New York, 1998).

[2] A. Lebed, *The Physics of Organic Superconductors and Conductors*, Springer Series in Materials Science (Springer, Berlin, Heidelberg, 2008).

[3] H. Seo, C. Hotta, and H. Fukuyama, Toward systematic understanding of diversity of electronic properties in low-dimensional molecular solids, Chem. Rev. **104**, 5005 (2004).

[4] D. Jérome, Organic conductors: From charge density wave TTF-TCNQ to superconducting $\mathrm{(TMTSF)_2PF_6}$, Chem. Rev. **104**, 5565 (2004).

[5] S. E. Brown, P. M. Chaikin, and M. J. Naughton, La tour des sels de bechgaard, in *The Physics of Organic Superconductors and Conductors*, edited by A. Lebed (Springer, Berlin, Heidelberg, 2008), pp. 49–87.

[6] D. Jérome, A. Mazaud, M. Ribault, and K. Bechgaard, Superconductivity in a synthetic organic conductor $\mathrm{(TMTSF)_2PF_6}$, J. Phys. Lett. **41**, 95 (1980).

[7] M. T. Béal-Monod, C. Bourbonnais, and V. J. Emery, Possible superconductivity in nearly antiferromagnetic itinerant fermion systems, Phys. Rev. B **34**, 7716 (1986).

[8] Y. Hasegawa and H. Fukuyama, NMR relaxation time of the anisotropic superconducting state in quasi-one-dimensional systems, J. Phys. Soc. Jpn. **56**, 877 (1987).

[9] M. Takigawa, H. Yasuoka, and G. Saito, Proton spin relaxation in the superconducting state of $\mathrm{(TMTSF)_2ClO_4}$, J. Phys. Soc. Jpn. **56**, 873 (1987).

[10] H. Shimahara, Long-range spin-fluctuations and superconductivity in quasi-one-dimensional organic compounds, J. Phys. Soc. Jpn. **58**, 1735 (1989).

[11] S. E. Brown, Organic superconductors: The Bechgaard salts and relatives, Physica (Amsterdam) **514C**, 279 (2015).

[12] D. S. Chow, F. Zamborszky, B. Alavi, D. J. Tantillo, A. Baur, C. A. Merlic, and S. E. Brown, Charge Ordering in the TMTTF Family of Molecular Conductors, Phys. Rev. Lett. **85**, 1698 (2000).

[13] S. Kitou, L. Zhang, T. Nakamura, and H. Sawa, Complex changes in structural parameters hidden in the universal phase diagram of the quasi-one-dimensional organic conductors $\mathrm{(TMTTF)_2}X$ ($X = \mathrm{NbF_6}$, $\mathrm{AsF_6}$, $\mathrm{PF_6}$, and Br), Phys. Rev. B **103**, 184112 (2021).

[14] H. Seo and H. Fukuyama, Antiferromagnetic phases of one-dimensional quarter-filled organic conductors, J. Phys. Soc. Jpn. **66**, 1249 (1997).

[15] H. Seo, Charge ordering in organic ET compounds, J. Phys. Soc. Jpn. **69**, 805 (2000).

[16] B. J. Powell and R. H. McKenzie, Strong electronic correlations in superconducting organic charge transfer salts, J. Phys. Condens. Matter **18**, R827 (2006).

[17] F. Zamborszky, W. Yu, W. Raas, S. E. Brown, B. Alavi, C. A. Merlic, and A. Baur, Competition and coexistence of bond and charge orders in $\mathrm{(TMTTF)_2AsF_6}$, Phys. Rev. B **66**, 081103(R) (2002).

[18] F. Iwase, K. Sugiura, K. Furukawa, and T. Nakamura, $^{13}\mathrm{C}$ NMR study of the magnetic properties of the quasi-one-dimensional conductor $\mathrm{(TMTTF)_2SbF_6}$, Phys. Rev. B **84**, 115140 (2011).

[19] M. Dressel, M. Dumm, T. Knoblauch, and M. Masino, Comprehensive optical investigations of charge order in organic chain compounds $\mathrm{(TMTTF)_2X}$, Crystals **2**, 528 (2012).

[20] M. Kuwabara, H. Seo, and M. Ogata, Coexistence of charge order and spin–peierls lattice distortion in one-dimensional organic conductors, J. Phys. Soc. Jpn. **72**, 225 (2003).

[21] M. Sugiura, M. Tsuchiizu, and Y. Suzumura, Spin-peierls transition temperature in quarter-filled organic conductors, J. Phys. Soc. Jpn. **74**, 983 (2005).

[22] K. Yoshimi, H. Seo, S. Ishibashi, and S. E. Brown, Tuning the Magnetic Dimensionality by Charge Ordering in the Molecular TMTTF Salts, Phys. Rev. Lett. **108**, 096402 (2012).

[23] R. T. Clay and S. Mazumdar, From charge- and spin-ordering to superconductivity in the organic charge-transfer solids, Phys. Rep. **788**, 1 (2019).

[24] H. Yoshioka, Y. Otsuka, and H. Seo, Theoretical studies on phase transitions in quasi-one-dimensional molecular conductors, Crystals **2**, 996 (2012).

[25] M. Dumm, A. Loidl, B. W. Fravel, K. P. Starkey, L. K. Montgomery, and M. Dressel, Electron spin resonance studies on the organic linear-chain compounds $(\mathrm{TMT}C\mathrm{F})_2X$ $C = \mathrm{S}$, Se; $X = \mathrm{PF}_6$, AsF_6, ClO_4, Br), Phys. Rev. B **61**, 511 (2000).

[26] M. Sakata, Y. Yoshida, M. Maesato, G. Saito, K. Matsumoto, and R. Hagiwara, Preparation of superconducting $(\mathrm{TMTSF})_2\mathrm{NbF}_6$ by electrooxidation of TMTSF using ionic liquid as electrolyte, Mol. Cryst. Liq. Cryst. **452**, 103 (2006).

[27] A. Rohwer, M. Dressel, and T. Nakamura, Deuteration effects on the transport properties of $(\mathrm{TMTTF})_2X$ salts, Crystals **10**, 1085 (2020).

[28] B. Köhler, E. Rose, M. Dumm, G. Untereiner, and M. Dressel, Comprehensive transport study of anisotropy and ordering phenomena in quasi-one-dimensional $(\mathrm{TMTTF})_2X$ salts ($X = \mathrm{PF}_6$, AsF_6, SbF_6, BF_4, ClO_4, ReO_4), Phys. Rev. B **84**, 035124 (2011).

[29] See Supplemental Material at http://link.aps.org/supplemental/10.1103/PhysRevLett.131.036401 for details of experimental data and microscopic parameters in *ab initio* Hamiltonians, and the explanation of the screened Coulomb interaction trends and their effects on the electronic state, which includes Refs. [30–33].

[30] N. Thorup, G. Rindorf, H. Soling, and K. Bechgaard, The structure of di(2,3,6,7-tetramethyl-1,4,5,8-tetraselenafulvalenium) hexafluorophosphate, $(\mathrm{TMTSF})_2\mathrm{PF}_6$, the first superconducting organic solid, Acta Crystallogr. Sect. B **37**, 1236 (1981).

[31] F. Wudl, Three-dimensional structure of the superconductor $(\mathrm{TMTSF})_2\mathrm{AsF}_6$ and the spin-charge separation hypothesis, J. Am. Chem. Soc. **103**, 7064 (1981).

[32] M. Sakata, Y. Yoshida, M. Maesato, G. Saito, K. Matsumoto, and R. Hagiwara, Preparation of superconducting $(\mathrm{TMTSF})_2\mathrm{NbF}_6$ by electrooxidation of TMTSF using ionic liquid as electrolyte, Mol. Cryst. Liq. Cryst. **452**, 103 (2006).

[33] https://isspns-gitlab.issp.u-tokyo.ac.jp/k-yoshimi/tm-salts.

[34] K. Momma and F. Izumi, VESTA 3 for three-dimensional visualization of crystal, volumetric and morphology data, J. Appl. Crystallogr. **44**, 1272 (2011).

[35] Y. Nogami, T. Ito, K. Yamamoto, N. Irie, S. Horita, T. Kambe, N. Nagao, K. Oshima, N. Ikeda, and T. Nakamura, X-ray structural study of charge and anion orderings of TMTTF salts, J. Phys. IV (France) **131**, 39 (2005).

[36] P. Hohenberg and W. Kohn, Inhomogeneous electron gas, Phys. Rev. **136**, B864 (1964).

[37] W. Kohn and L. J. Sham, Self-consistent equations including exchange and correlation effects, Phys. Rev. **140**, A1133 (1965).

[38] D. Tahara and M. Imada, Variational Monte Carlo method combined with quantum-number projection and multi-variable optimization, J. Phys. Soc. Jpn. **77**, 114701 (2008).

[39] T. Misawa, S. Morita, K. Yoshimi, M. Kawamura, Y. Motoyama, K. Ido, T. Ohgoe, M. Imada, and T. Kato, mVMC—Open-source software for many-variable variational Monte Carlo method, Comput. Phys. Commun. **235**, 447 (2019).

[40] https://www.pasums.issp.u-tokyo.ac.jp/mvmc/en/.

[41] P. Giannozzi, O. Andreussi, T. Brumme, O. Bunau, M. B. Nardelli, M. Calandra, R. Car, C. Cavazzoni, D. Ceresoli, M. Cococcioni *et al.*, Advanced capabilities for materials modelling with quantum ESPRESSO, J. Phys. Condens. Matter **29**, 465901 (2017).

[42] D. R. Hamann, Optimized norm-conserving Vanderbilt pseudopotentials, Phys. Rev. B **88**, 085117 (2013).

[43] M. Schlipf and F. Gygi, Optimization algorithm for the generation of ONCV pseudopotentials, Comput. Phys. Commun. **196**, 36 (2015).

[44] J. P. Perdew, K. Burke, and M. Ernzerhof, Generalized Gradient Approximation Made Simple, Phys. Rev. Lett. **77**, 3865 (1996).

[45] S. Ishibashi, First-principles electronic-band calculations on organic conductors, Sci. Technol. Adv. Mater. **10**, 024311 (2009).

[46] F. Aryasetiawan, M. Imada, A. Georges, G. Kotliar, S. Biermann, and A. I. Lichtenstein, Frequency-dependent local interactions and low-energy effective models from electronic structure calculations, Phys. Rev. B **70**, 195104 (2004).

[47] M. Imada and T. Miyake, Electronic structure calculation by first principles for strongly correlated electron systems, J. Phys. Soc. Jpn. **79**, 112001 (2010).

[48] H. Shinaoka, T. Misawa, K. Nakamura, and M. Imada, Mott transitionand phase diagram of κ-$(\mathrm{BEDT\text{-}TTF})_2\mathrm{Cu(NCS)}_2$ studied by two-dimensional model derived from *Ab initio* method, J. Phys. Soc. Jpn. **81**, 034701 (2012).

[49] T. Misawa, K. Yoshimi, and T. Tsumuraya, Electronic correlation and geometrical frustration in molecular solids: A systematic *ab initio* study of β'-$X[\mathrm{Pd(dmit)}_2]_2$, Phys. Rev. Res. **2**, 032072(R) (2020).

[50] K. Yoshimi, T. Tsumuraya, and T. Misawa, *Ab initio* derivation and exact diagonalization analysis of low-energy effective Hamiltonians for β'-$\mathrm{X}[\mathrm{Pd(dmit)}_2]_2$, Phys. Rev. Res. **3**, 043224 (2021).

[51] K. Ido, K. Yoshimi, T. Misawa, and M. Imada, Unconventional dual 1D-2D quantum spin liquid revealed by *ab initio* studies on organic solids family, npj Quantum Mater. **7**, 48 (2022).

[52] D. Ohki, K. Yoshimi, and A. Kobayashi, Interaction-induced quantum spin Hall insulator in the organic Dirac electron system α-$(\mathrm{BEDT\text{-}TSeF})_2\mathrm{I}_3$, Phys. Rev. B **105**, 205123 (2022).

[53] D. Ohki, K. Yoshimi, and A. Kobayashi, Transport properties of the organic Dirac electron system α-$(\mathrm{BEDT\text{-}TSeF})_2\mathrm{I}_3$, Phys. Rev. B **102**, 235116 (2020).

[54] K. Nakamura, Y. Yoshimoto, Y. Nomura, T. Tadano, M. Kawamura, T. Kosugi, K. Yoshimi, T. Misawa, and Y. Motoyama, RESPACK: An *ab initio* tool for derivation of effective low-energy model of material, Comput. Phys. Commun. **261**, 107781 (2021).

[55] K. Yoshimi, H. Seo, S. Ishibashi, and S. E. Brown, Spin frustration, charge ordering, and enhanced antiferromagnetism in $\mathrm{TMTTF_2SbF_6}$, Physica (Amsterdam) **407B**, 1783 (2012).

[56] A. C. Jacko, H. Feldner, E. Rose, F. Lissner, M. Dressel, R. Valentí, and H. O. Jeschke, Electronic properties of fabre charge-transfer salts under various temperature and pressure conditions, Phys. Rev. B **87**, 155139 (2013).

[57] M. C. Gutzwiller, Effect of Correlation on the Ferromagnetism of Transition Metals, Phys. Rev. Lett. **10**, 159 (1963).

[58] R. Jastrow, Many-body problem with strong forces, Phys. Rev. **98**, 1479 (1955).

[59] S. Sorella, Generalized Lanczos algorithm for variational quantum Monte Carlo, Phys. Rev. B **64**, 024512 (2001).

[60] K. Nakamura, Y. Yoshimoto, Y. Nohara, and M. Imada, *Ab initio* low-dimensional physics opened up by dimensional downfolding: Application to LaFeAsO, J. Phys. Soc. Jpn. **79**, 123708 (2010).

[61] K. Nakamura, Y. Yoshimoto, and M. Imada, *Ab initio* two-dimensional multiband low-energy models of $\mathrm{EtMe_3Sb[Pd(dmit)_2]_2}$ and κ-$(\mathrm{BEDT\text{-}TTF})_2\,\mathrm{Cu(NCS)_2}$ with comparisons to single-band models, Phys. Rev. B **86**, 205117 (2012).